Supporting Information

Single-sided NMR to estimate morphological parameters of the trabecular bone structure

Marco Barbieri[1,2], Paola Fantazzini[1], Villiam Bortolotti[3], Fabio Baruffaldi[4], Anna Festa[4], David N. Manners[5], Claudia Testa[1,6], Leonardo Brizi[1,6]

[1] University of Bologna, Physics and Astronomy Department, Viale Berti Pichat 6/2 40127, BO, Italy
[2] Stanford University, Department of Radiology, 1201 Welch Rd, Stanford, 94305, CA, USA
[3] Department of Civil, Chemical, Environmental, and Materials Engineering, University of Bologna, Italy
[4] IRCCS Istituto Ortopedico Rizzoli, Via di Barbiano 1/10, 40136 Bologna, Italy
[5] Department of Biomedical and Neuromotor Sciences, University of Bologna, Italy
[6] INFN Bologna, Bologna, Italy.

Sketch of the NMR-MOUSE PM10 and the signal acquisition procedure

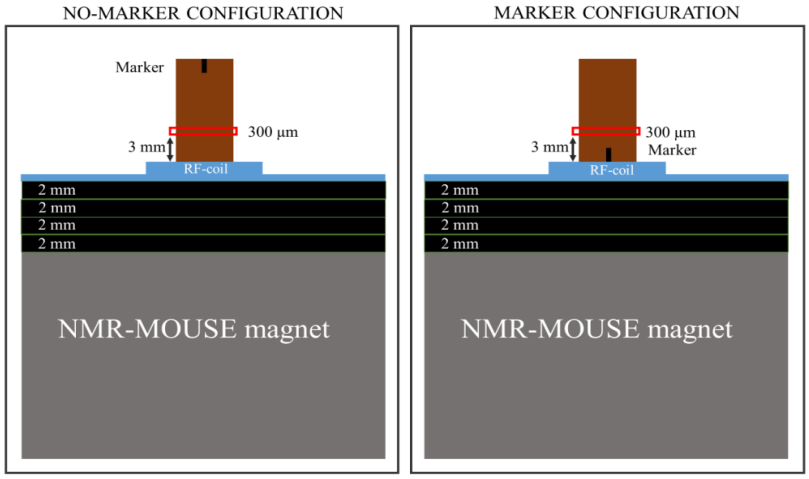

Figure S1. Depiction of the signal acquisition procedure using the NMR-MOUSE PM10. Four spacers (each 2 mm thick) were used to optimize the Signal to Noise Ratio (SNR). The sensitive volume was 3 mm from the surface coil, and its thickness was 300 μm with a base area of 1.5 x 1.5 cm^2, determined by the size of the RF coil. NMR measurements were carried out on the two ends of each cylindrical sample: one with the marked face away from the r.f. coil (No-Marker Configuration) and one with the marked face close to the coil (Marker Configuration).

Examples of micro-CT images, image histograms and binary images for three samples that represent three different conditions found in our set of bone samples (cored from the humeral head)

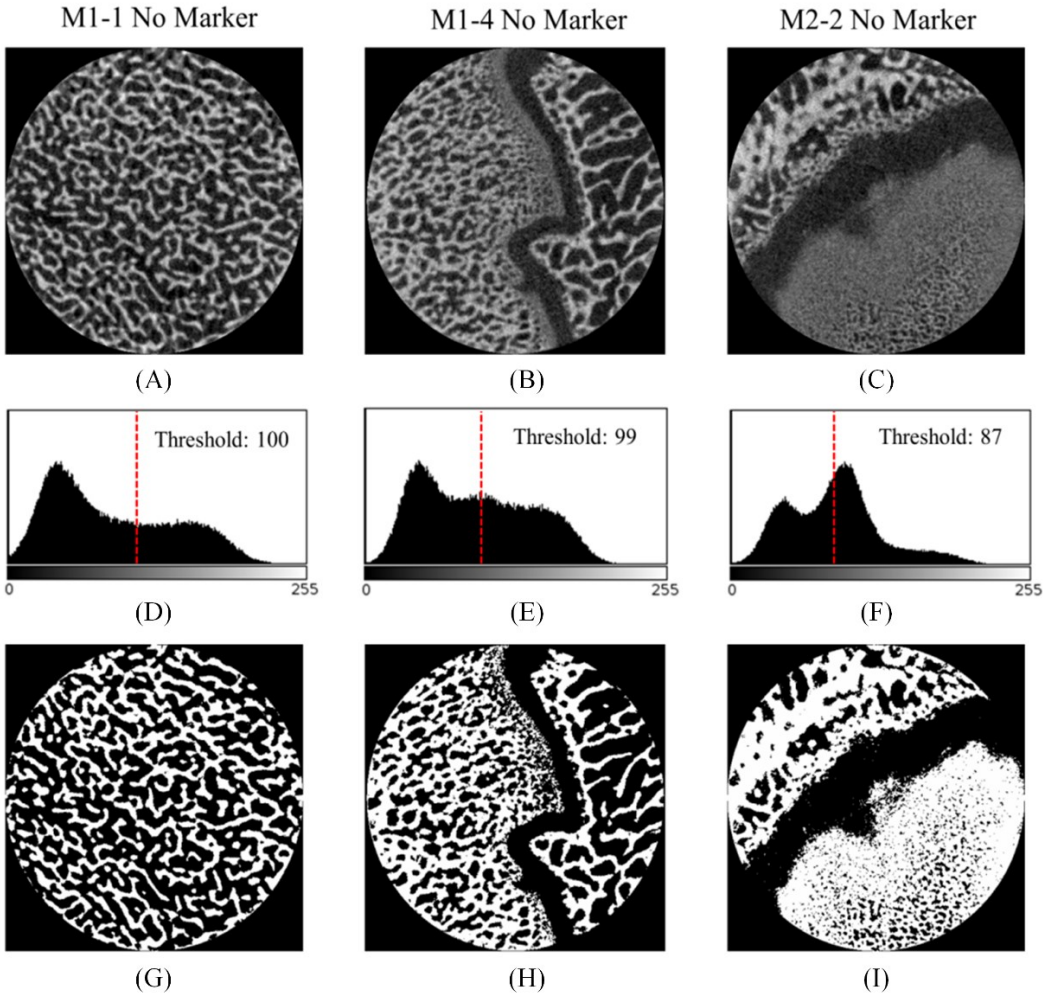

Figure S2. Examples of micro-CT images (top), image histograms (middle) and binary images obtained after global thresholding by Otsu's method (bottom) for the slices of three samples. For each sample, a micro-CT image of an acquired slice is reported along with its histogram and binary image. (A), (D) and (G) refer to sample M1-1-No-Marker, in which only bone and marrow tissues were present; (B), (E) and (H) to sample M1-4-No-Marker, in which growth cartilage and less mineralized bone tissues were present in addition to marrow and bone tissues; (C), (F) and (I) to sample M2-2-No-Marker, in which growth cartilage and less mineralized bone tissues were present in addition to marrow and bone tissues, and the less mineralized bone dominated the image. The image histogram of sample M1-1-No-Marker shows one low peak, which represents the bone marrow, a high peak represents the bone tissue, and a flat transition between. For sample M2-2-No-Marker, the low intensity peak incorporates both bone marrow and growth cartilage (appearing dark in the micro-CT image), and between this and the high intensity shoulder, a third peak is present in place of the flat transition, due to bone characterized by reduced mineralization compared to fully calcified bone, as evidenced by the lower gray level. In sample M1-4-No-Marker, where less mineralized bone is present, the third histogram peak is barely visible, and the transitional portion almost flat.

Effect of the different thresholds to binarize micro-CT images on the micro-CT estimates of BV/TV

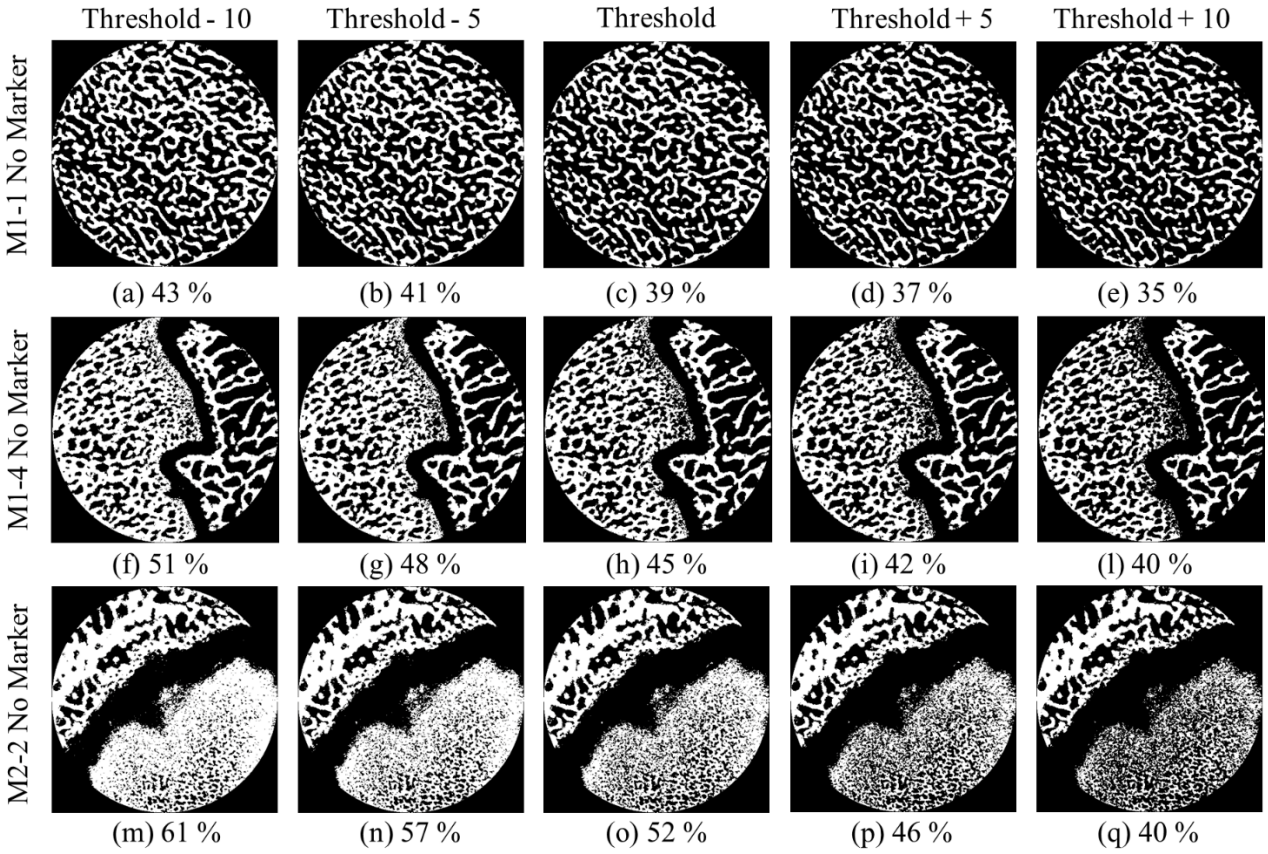

Figure S3. Examples showing the effect on *BV/T*V estimates using 5 different gray level threshold values. "Optimal" threshold values estimated by Otsu's method are 100 for M1-1-No-Marker (first row), 99 for M1-4-No-Marker (second row) and 87 for M2-2-No-Marker (third row). Five values bracketing the "optimal threshold value" are shown. Estimated *BV/TV* values are written below the corresponding images. For samples M1-1-No-Marker and M1-4-No-Marker there is a linear relationship between the threshold values and the corresponding *BV/TV* values. On the contrary, for the sample M2-2-No-Marker, characterized by less mineralized bone, the variation is not linear. Increasing or decreasing the threshold up to 10 gray levels respect to the Otsu's value, produces asymmetrical change in the *BV/TV* estimates. This effect was also found for sample M2-4-Marker (not shown), which likewise showed a relative high proportion of less mineralized bone tissue.

Inversion from experimental NMR CPMG data to quasi-continuous and discrete T_2 distributions

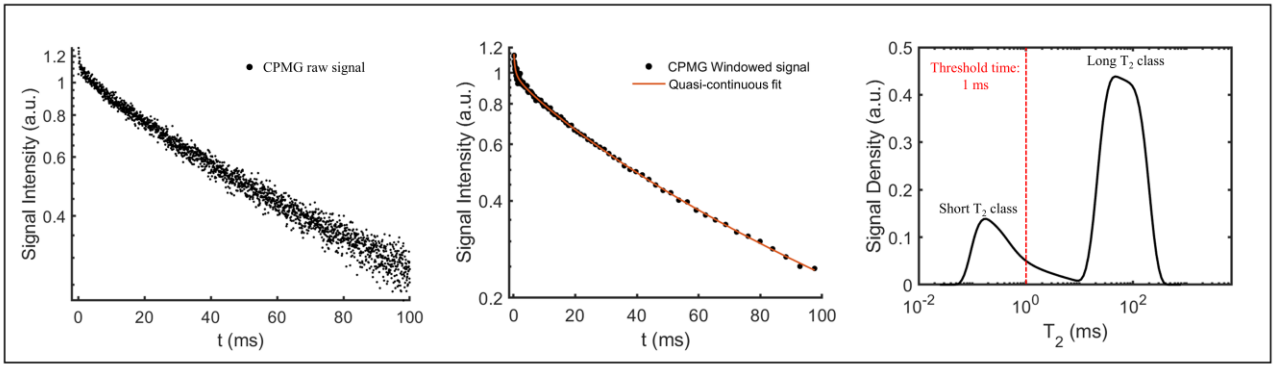

(A)

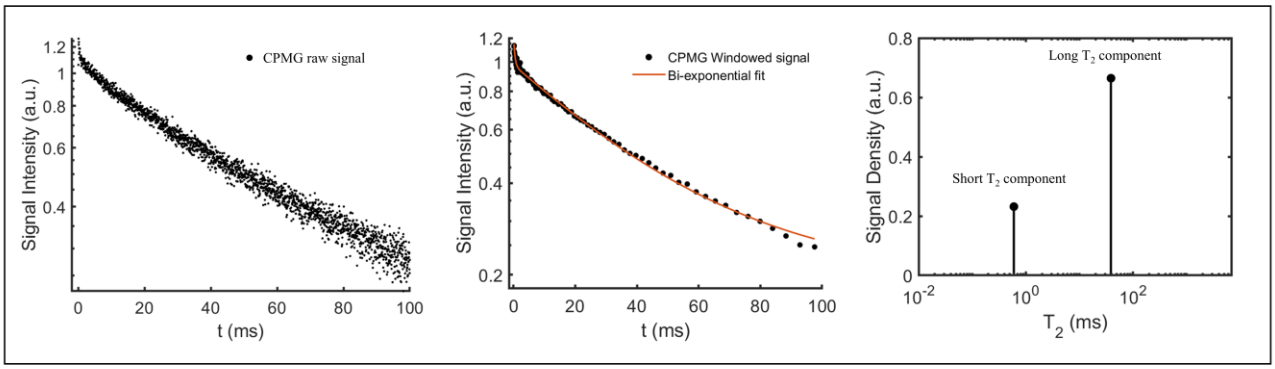

(B)

Pipeline for the analysis of the CPMG decay curves using (A) Inverse Laplace Transform to obtain a T_2 quasi-continuous distribution using UpenWin software; the fit to the CPMG windowed data is obtained by the transformation of the quasi-continuous distribution back into the time domain, and (B) bi-exponential fits. Noise reduction through windowing of raw data was performed for both inversions. In the order, for both methods from left to right: raw data, windowed data with matched fit data, and finally, T_2 quasi-continuous or two-component distributions, respectively. Firstly, windowing was done to reduce the size of the data set and to de-noise the data. For the first few data points of the decay no average was performed to avoid suppression of fast decay processes. The window was then translated through the decay curve and the length of the window as progressively increased until it reached a fixed maximum length.

Principal Component Analysis of micro-CT parameters

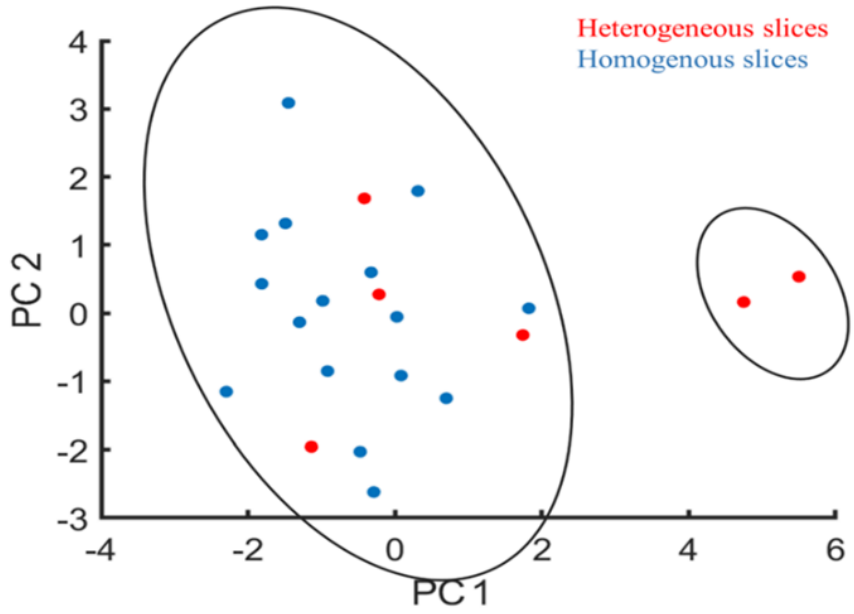

Figure S5. Scatter plot of the first two principal components of a principal component analysis (PCA) of the set of animal trabecular bone samples examined. Each sample was characterized by a feature vector composed of the normalized morphological parameters evaluated by micro-CT. Two groups were clearly separable. Red dots mark the samples in which growth cartilage and less mineralized bone tissue were present (Figure 1 from (D) to (I)). The less populated cluster contains the two samples characterized by the highest tissue heterogeneity: "M2-2 No Marker" and "M2-4 Marker" (Figure 1 (G) and (I)). These two samples, having negative *Tb.Pf.* in Table 2, were therefore excluded from the comparison between NMR and micro-CT results.

Comparison between intra-trabecular porosity values found in this study and those reported in literature

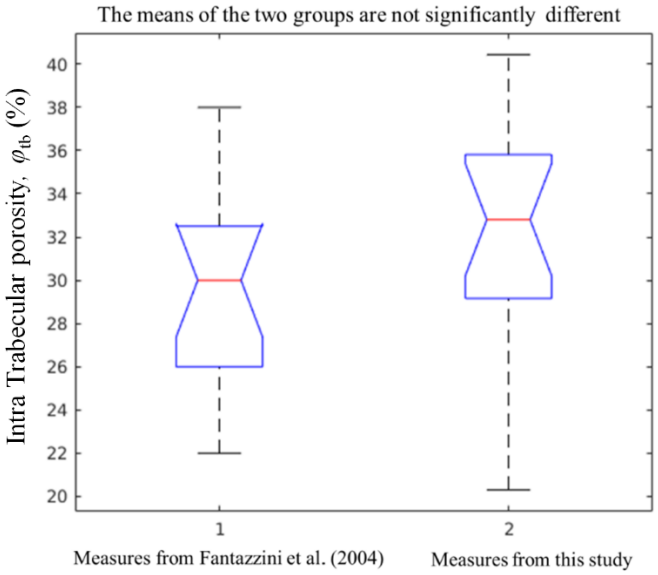

Figure S6. Box plots of the intra-trabecular porosity values reported in Ref. [19] and those found in this study. The difference of the two means was not significant (p = 0.12). It is worth nothing that different methods of sample preparation and NMR data acquisition were adopted in the two studies. In Ref. [19] samples were defatted, water saturated, while the NMR data were T_1 distributions estimated from Inversion Recovery, acquired on a homogeneous magnetic field relaxometer. In both cases the intra-trabecular porosity was estimated by intra- and inter-trabecular signal separation.

NMR Data analysis using the quasi-continuous distribution and the bi-components T_2 distributions

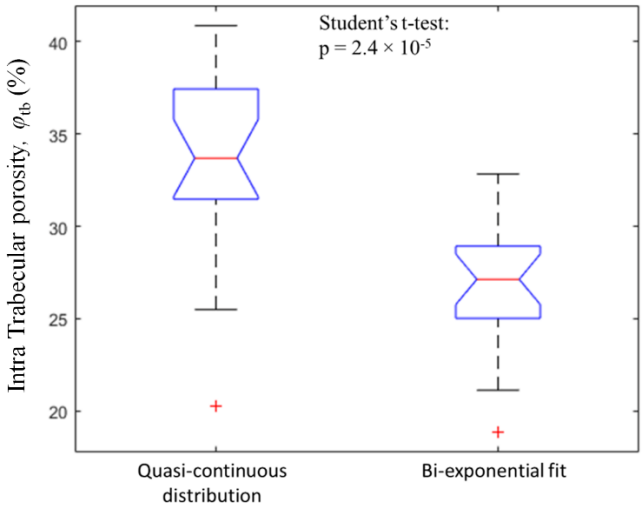

Figure S7. Box plots of the intra-trabecular porosity values found in this study using the quasi-continuous distribution of relaxation times and the bi-exponential fit. The means of the two groups of values differed significantly based on the t-test ($p = 2.4 \times 10^{-5}$).

Comparison between NMR and micro-CT estimated parameters BV/TV and BS/TV, by applying bi-exponential fits to the CPMG data.

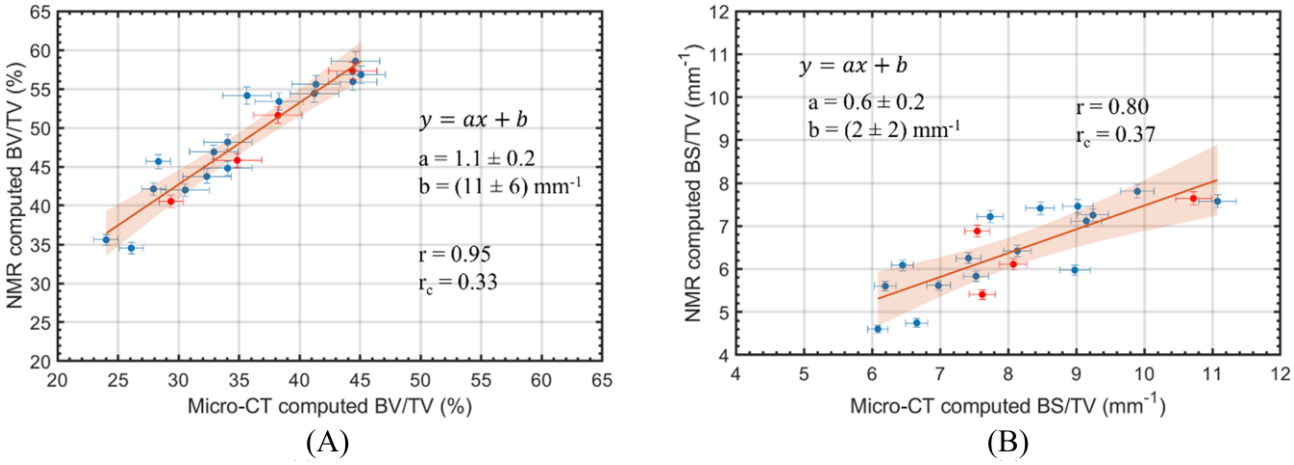

Figure S8. Comparison of parameters computed using micro-CT or by NMR, applying bi-component fits to the CPMG data. For each sample, the group means of intra-trabecular porosity (27%) and half the average trabecular thickness (86 µm) were used as values of φ_{tb} and R in Eq. 5 and 7 to compute *BV/TV* and *BS/TV* ratios, respectively. Although strong correlations with the ground-truth values were found for both NMR-estimated *BV/TV* and *BS/TV*, the agreement of NMR with micro-CT values was only weak to moderate. For *BV/TV*, Pearson's coefficient was $r = 0.95$, but Lin's coefficient was 0.33, which is considerably less than the Lin's coefficient found when the quasi-continuous T_2 distribution was used to separate intra- and inter-trabecular signals. The low-moderate agreement is determined mainly by the bias term of the linear fit, which is (11 ± 6) %, whereas the slope is 1.1 ± 0.2. For the *BS/TV* ratio, Pearson's coefficient was $r = 0.80$ but the Lin's coefficient was 0.37. The slope of the linear fit was 0.6 ± 0.2, whereas the bias term was (2 ± 2) mm^{-1}. With the two-component fits some of the components with T_2 >1 ms are assigned to the short T_2 component, with the effect of assigning signal from the inter-trabecular spaces to the intra-trabecular compartment. This leads to an overestimation of the trabecular volume, which explains why NMR *BV/TV* values overestimate the micro-CT values (Figure S8A). It is also interesting to note that in this case, the four samples containing cartilage do not fall below the best-fit line. This is because T_2 relaxation times of the cartilage are in the order of tens of ms [13], which is the same order of magnitude as the T_2 relaxation times of the marrow. Hence, the cartilage signal, being part of the long T_2 component, assumed to be inter-trabecular, does not contribute to the estimated trabecular volume. Likewise, in micro-CT images, growth cartilage has gray level intensities similar to bone marrow, and does not contribute to estimated trabecular volume.

BV/TV and BS/TV estimations: minimization of the mean squared error between NMR and micro-CT estimators, by applying bi-exponential fits to the CPMG data

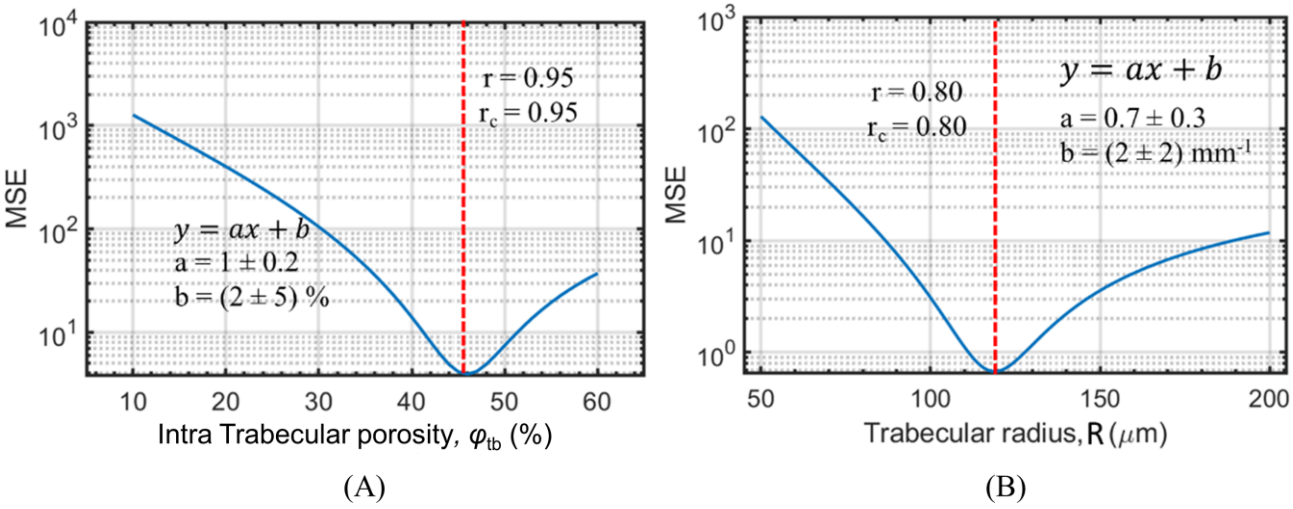

Figure S9. Minimization of the mean squared error (MSE) between NMR and micro-CT estimates as a function of φ_{tb} and trabecular radius R. (A) MSE between NMR and micro-CT computed *BV/TV* as a function of the free parameter φ_{tb} in Eq. 5. (B) MSE between NMR and micro-CT computed *BS/TV* as a function of the free parameter trabecular radius R in Eq.7. The best value for φ_{tb} was found to be 46%, which is considerably higher than the measured mean intra trabecular porosity, and it is also considerably higher than the value reported in [19]. The best trabecular radius was found to be ≈ 130 μm, which is considerably higher than the expected average value for the radius, which was estimated as 86 μm by the micro-CT analysis. The linear regressions and the corresponding coefficients represented inside the figures have the same meaning as in Figure 5, Figure 7 and Figure S8.

References

[13] Barbieri M, Brizi L, Bortolotti V, et al. Single-sided NMR for the diagnosis of osteoporosis: Diffusion weighted pulse sequences for the estimation of trabecular bone volume fraction in the presence of muscle tissue. Microporous and Mesoporous Materials. 2018;269:166-170. doi:10.1016/j.micromeso.2017.05.023.

[19] Fantazzini P, Bortolotti V, Brown RJS, et al. Two ^{1}H-nuclear magnetic resonance methods to measure internal porosity of bone trabeculae: By solid–liquid signal separation and by longitudinal relaxation. Journal of Applied Physics. 2004;95(1):339-343. doi:10.1063/1.1630374.